GAS AND DARK MATTER SPHERICAL DYNAMICS

Jean-Pierre Chièze, Romain Teyssier
CEA, DSM/DAPNIA/Service d'Astrophysique, CE-Saclay, F-91191 Gif-sur-Yvette, Cedex, France

Jean-Michel Alimi
Laboratoire d'Astrophysique Extragalactique et de Cosmologie, CNRS URA 173, Observatoire de Paris-Meudon, 92195 Meudon, France

ABSTRACT

We investigate the formation of spherical cosmological structures following both dark matter and gas components. We focus on the dynamical aspect of the collapse assuming an adiabatic, $\gamma = 5/3$, fully ionized primordial plasma. We use for that purpose a fully Lagrangian hydrodynamical code designed to describe highly compressible flows in spherical geometry. We investigate also a "fluid approach" to describe the mean physical quantities of the dark matter flow. We test its validity for a wide range of initial density contrast. We show that an homogeneous isentropic core forms in the gas distribution, surrounded by a self-similar hydrostatic halo, with much higher entropy generated by shock dissipation. We derive analytical expressions for the size, density and temperature of the core, as well as for the surrounding halo. We show that, unless very efficient heating processes occur in the intergalactic medium, we are unable to reproduce within adiabatic models the typical core sizes in X-ray clusters. We also show that, for dynamical reasons only, the gas distribution is naturally *antibiased* relative to the total mass distribution, without invoking any reheating processes. This could explain why the gas fraction increases with radius in very large X-ray clusters. As a preparation for the next study devoted to the thermodynamical aspect of the collapse, we investigate the initial entropy level required to solve the core problem in X-ray clusters.

Subject headings: Cosmology: theory – dark matter – galaxy formation – hydrodynamics – methods: numerical

1. INTRODUCTION

This paper is the first in a series devoted to the hydrodynamical study of the formation of structures in cosmology. We focus here on a precise description of the dynamics of dark matter and gas collapse. Non adiabatic processes, namely temperature decoupling between the various plasma components, heat conduction, non equilibrium ionization balance, cooling, heating by star formation are examined in a following paper (Chièze, Teyssier & Alimi 1997).

Gas and dark matter distributions observed in X-ray clusters provides strong constraints on structure formation theory. Although the gas density profile shows in the most massive clusters a typical core–halo structure (Hughes 1989; Briel, Henry & Bohringer 1992), the total mass distribution deduced from lensing analysis seems to be strongly peaked towards the center, with no clear evidence of a central core. EINSTEIN and ROSAT observations of X-ray clusters show gas core radii with sizes ranging from 100 to 300 h^{-1} kpc. Recent studies of gravitational lensing in clusters suggest that the total mass distribution can be singular

in the center (Wu & Hammer 1993 and reference therein) or at least with very small core radii ($r_{core} \simeq$ 20-30 h^{-1} kpc) (Tyson, Valdez & Wenk 1990; Mellier et al. 1994; Flores & Primack 1996). Moreover, gas and dark matter distribution differ also in the outer parts of galaxy clusters. David, Jones & Forman (1995) (hereafter DJF) show that there is a strong *antibias* of the X-ray gas in the clusters with respect to the underlying total mass distributions. The gas mass fraction increases with radius, up to what should be the primordial gas fraction $\Omega_B/\Omega_0 \simeq 0.2 - 0.3$ (White et al. 1993). The origin of such an antibias is an open question. A model of cluster formation, which takes into account the dynamics of both dark and gas component, should be able to reproduces these features.

The most rigorous approach so far of the coupled gas and dark matter dynamics was performed by Bertschinger (1985) in the case of the self-similar secondary infall. Its analysis showed that the final gas distribution traces the dark matter distribution. For more general initial conditions, it is generally admitted that such a conclusion subsists as long as thermal processes are not included. More recent studies, based essentially on 3D numerical simulations of structure formation, show however that gas and dark matter have different distributions due to the hierarchical nature of gravitational clustering. Antibiasing is due to a systematic energy transfer from dark matter to gas during mergers of protoclusters (Navarro & White 1993; Pearce, Thomas & Couchman 1994). We propose to address again this question, by considering first the role of the purely adiabatic dynamics (this paper), and second the role of various thermal processes (Chièze, Teyssier & Alimi 1997) with a high resolution hydrodynamical treatment.

The hierarchical nature of gravitational collapse requires, in principle, high resolution, 3D simulations. But it is difficult to reconcile physical completeness with topological realism. Plain hydrodynamics simulations generally suffer from limited resolution and reduced physical inputs, while one-dimensional calculations offer a practically unlimited resolution, with however a highly constrained and unrealistic geometry. They are also useful tools to work out and reveal the potential effects of various physical processes. Moreover, accurate numerical methods can be more easily refined in 1D models, especially in a high resolution Lagrangian framework, and then provides a valuable complement to more elaborated 3D simulations of the formation of large–scale structures.

The object of this paper is to study the gas and dark matter dynamics, with a one dimensional, high resolution, Lagrangian model, in a way similar to Thoul & Weinberg (1995) in spherical geometry or to Shapiro & Struck-Marcell (1984) in slab geometry. In the spherical case presented in this paper, we focus on the differences between gas and dark matter distributions due to dynamical processes only. In order to understand clearly the dynamical features of both components, it appears more convenient to consider separately the pure gas and the pure dark matter collapse, before investigating the coupled dynamics.

When the calculation of the pure gas collapse of a perturbed spherical system is worked out along these lines, it appears that the collapse of the inner regions actually proceeds to very high densities. This is due to the fact that - given any reasonable density perturbation - the inner subsonic flow is not far from homologous, so that shock heating has here little effects. More precisely, it exists a central core which evolves strictly adiabatically up to hydrostatic equilibrium. This core is bounded by the sonic radius (where the gas velocity is equal to the sound velocity), from which the accretion shock originates and propagates outward. The final central density depends on the core initial entropy. We develop in Section 2.2 an analytical model which describes precisely the core structure and the surrounding halo. Section 2.3 presents results of numerical simulations which confirm both the numerical model developed in section 2.1 and the previous analytical model of a pure gas collapse.

The collapse of collisionless dark matter is supposed to provide the potential well in which gas is falling,

and thus deserves special attention. The very high dynamical range required for the treatment of the gas component claims for an equivalent dynamical range in the treatment of the collisionless component. A classical method, adapted to spherical geometry, consists in calculating the trajectories of concentric shells of collisionless material. However, it appears rapidly that the numerical accuracy which can be achieved with this method cannot, for any reasonable computing time, meet the very stringent dynamical range and resolution requirements imposed by the gas evolution. First, the dark matter distribution in each Lagrangian gas element must be well sampled by a sufficient number of dark matter shells, which requires a very large number of shells, with no guarantee of a smooth dark matter distribution. Second, the mass distribution must be calculated over more than 10 decades in radius. In view of these difficulties, we propose in Section 3 a "fluid model" for the dark matter component, which very accurately accounts for its gravitational behavior. In this way, the collisional and collisionless components are treated on an equal numerical footing.

The resulting coupled model contains all the dynamical aspects of the spherical collapse of both gas and dark matter. Some salient features of this model are discussed in Section 4. We show that for purely dynamical reasons the gas and dark matter distributions differ significantly, leading to an *antibiased* gas distribution relative to the total gravitational mass. We investigate the influence of the baryons density parameter on the gas distribution and we compare our results with the observational data of DJF, finding excellent agreements between our model and the most massive X-ray clusters. The difficulty to form realistic cores, even in adiabatic conditions, are finally discussed, in order to evaluate the initial entropy level required to explain the observed sizes of X-ray clusters core radii. It turned out that photo–ionization processes are not sufficient, and that galactic winds are good candidates to transfer enough energy to the intergalactic medium and solve the problem. The more complex and richer thermodynamical aspects of cosmic structure formation are discussed in a forthcoming paper (Chièze, Teyssier & Alimi 1997).

2. GAS DYNAMICS

In this section, we analyze the basic properties of the dissipative heating of the gas during gravitational collapse. The adiabatic dynamics does not depend on the ionization degree of matter. The gas is here assumed to be fully ionized, composed of 76% hydrogen and 24% helium by mass. We consider here the gravitational collapse of a purely gaseous, gravitationally bound, sphere. Emphasis is put on the treatment of shock waves, especially on the conditions of their appearance, both in time and space. Our high resolution Lagrangian treatment puts forward the formation of an adiabatic - isentropic - high density core, in which shocks never occurred. The importance of this core is that it determines the rest of the structure, essentially heated up by the dissipation of supersonic infall motions, in the relaxation layer of a moving accretion shock.

Mass motion kinetic energy is dissipated into heat across this shock by the action of viscous forces. The dissipative shock region has a characteristic width of a few particle mean free paths, generally well beyond the resolution of an hydrodynamical simulation. In most treatments, shock transitions are handled with a so-called "artificial viscosity" by which the entropy production rate is largely increased above its actual value, so that the shock width is spread over few cells. The success of the operation relies on the fact that Hugoniot-Rankine relations, which connect upstream and downstream gas properties (density, momentum and energy) are conservation relations, independent of the dissipative processes which drive the transition. However, it is essential to respect the correct dependency of the viscous force on the structure of the velocity field, in order to determine safely where and when in the flow "artificial" viscosity is

required. The viscous forces are described by the stress tensor, which, in spherical geometry, depends only on the combination $\left(\frac{\partial u}{\partial r} - \frac{u}{r}\right)$. As required, the stress vanishes for locally isotropic flows. This is of great importance for cosmological flows, which spend a long time close to uniform expansion or contraction.

We present briefly the main features of the numerical code we employed for this study. It is an evolution of a code which has been developed for various astrophysical purposes (Blottiau, Chièze & Bouquet 1988; de Boisanger, Chièze & Meltz 1992; Rothenflug *et al.* 1994).

In order to get very high resolution, the numerical scheme is Lagrangian. In all calculations presented here, the number of Lagrangian shells is 250, both for gas and dark matter. Since the resolution must be concentrated in the core, shell masses are distributed according to a geometrical progression, with a dynamical range of 10^{10}. For example, in the simulation of a 10^{16} $M_\odot$ cluster, the inner shell has a mass of 10^4 $M_\odot$ only, while the outer shells have a mass of 10^{14} $M_\odot$. It turns out that increasing the number of shells is unnecessary. The effective spatial resolution in the centre (in our case 0.1 pc) depends on the inner shell masses, not on the total number of shells, which just governs the resolution in the outer regions.

Numerical stability is guaranteed by a fully implicit method, which allows to retain the time step which limits the relative variations of the dependent variables to some small arbitrary value, generally 1% in the simulations presented here. The independent variables are the time t, and the cumulative mass m from the center. The dynamical dependent variables are the radius $r(m,t)$ of the sphere containing the mass m and the corresponding velocity $u(m,t)$. Dealing with perfect gases of adiabatic exponent $\gamma = 5/3$, the thermodynamical variable we adopt is the function

$$s(m,t) = \ln\left(EV^{\frac{1}{\gamma-1}}\right) \tag{1}$$

where E is the internal energy of a fluid element of volume V. The evolution of this thermodynamical function, reminiscent of the entropy, is given by

$$\frac{ds}{dt} = \frac{\dot{\mathcal{Q}}}{E} \tag{2}$$

where $\dot{\mathcal{Q}}$ is the variation rate of the internal energy due to dissipation or other thermal processes, excluding the work done by the *thermal* pressure. A choice of this nature is dictated by energy conservation considerations : it is clear that isentropic flows ($\dot{\mathcal{Q}} = 0$) numerically remain strictly isentropic, since we avoid the integration of the work done by pressure forces over the whole history of the system, which invariably introduces numerical inaccuracy. The internal boundary conditions are naturally $r\,(0,t) = 0$ and $u\,(0,t) = 0$ (no artificial core radius). Since the perturbation we study are always compensated, the velocity at the outer boundary is taken to be the unperturbed Hubble flow. Our study is devoted to adiabatic flows. Therefore, the dissipation term $\dot{\mathcal{Q}}$ is due to shock heating only. We now describe the form one should use for $\dot{\mathcal{Q}}$ in spherical geometry.

2.1. Dissipation in Shock Waves

We choose to handle shocks by the pseudo–viscosity method (PV method), introduced for planar shocks by Von Neumann & Richtmyer (1950). Though it is often considered as a numerical trick, this method has in fact firm physical grounds. In the PV method, the particle cross–section is reduced so that their mean

free–path matches the cell size of the simulation. Consequently, the PV method consists in solving correctly the Navier–Stokes (NS) equations with the available resolution, adapted in fact to a highly viscous flow. Note that the Hugoniot–Rankine relations, which connect the downstream to the upstream regions of an adiabatic shock, are independent of the detailed microphysics, since they just express conservation laws. This is the reason why the shock adiabats, calculated by the PV method, are strictly identical to those obtained by a NS calculation (see Chièze, Teyssier & Alimi 1997 for further comments).

In a fluid element, two distinct groups of time scales can be derived, related respectively to the microscopic properties of the plasma and to the macroscopic properties of the flow. In the first group, we find in particular the mean collision time τ_{coll} between particles, and the relaxation time τ_{rel} of the velocity distribution due to collisions. In the second group, two time scales characterize the rate at which the *shape* of the fluid element changes, and the rate at which its *volume* varies. The ratios of the time scales of different groups, $\tau_{(1)}/\tau_{(2)}$, measure the departure from thermodynamical equilibrium, which results in the apparition of a viscous stress of magnitude $\Pi \simeq p\ \tau_{(1)}/\tau_{(2)}$, where p is the thermodynamical pressure.

Departures from thermodynamical equilibrium resulting from the finite relaxation time of internal degrees of freedom, give rise to the so–called bulk viscosity. The corresponding scalar correction to the thermodynamical pressure is proportional to $\boldsymbol{\nabla} \cdot \boldsymbol{u}$. Since the relaxation time of the energy levels of atoms and ions ($\simeq 10^{-6}$s) is negligible compared to any relevant dynamical time scale pertinent to the problem, the bulk viscosity is absent.

The usual viscous stress tensor is related to the local rate of strain, that is, the rate at which the shape of a fluid element is altered. This means that locally isotropic motions can not generate any viscous stress. In Cartesian coordinates, the viscosity stress tensor, σ_{ij}, and the dissipation rate have the form (Landau & Lifshitz 1982)

$$\sigma_{ij} = -\eta \ \left(\frac{\partial u_i}{\partial x_j} + \frac{\partial u_j}{\partial x_i} - \frac{2}{3}\delta_{ij} \boldsymbol{\nabla} \cdot \boldsymbol{u} \right) \quad \text{and} \quad \dot{\mathcal{Q}} = \sigma_{ij} \frac{\partial u_i}{\partial x_j} \tag{3}$$

where η is the viscosity coefficient, proportional to the particles mean free–path. Since we are interested here in spherically symmetric flows, we recast these expressions into spherical coordinates

$$\sigma_{rr} = 2\eta \ \left(\frac{\partial u}{\partial r} - \frac{1}{3} \boldsymbol{\nabla} \cdot \boldsymbol{u} \right) \quad \text{and} \quad \sigma_{\theta\theta} = \sigma_{\phi\phi} = -\frac{1}{2}\ \sigma_{rr} \tag{4}$$

$$\dot{\mathcal{Q}} = \frac{3}{2} \sigma_{rr} \left(\frac{\partial u}{\partial r} - \frac{1}{3} \boldsymbol{\nabla} \cdot \boldsymbol{u} \right) = 3\eta \left(\frac{\partial u}{\partial r} - \frac{1}{3} \boldsymbol{\nabla} \cdot \boldsymbol{u} \right)^2 \tag{5}$$

The equation of motion has the form

$$\rho \frac{du}{dt} = -\frac{\partial P}{\partial r} - \rho \frac{\partial \Phi}{\partial r} + \frac{\partial \sigma_{rr}}{\partial r} + \frac{3}{r} \sigma_{rr} \tag{6}$$

where du/dt is the material acceleration of the fluid. This formulation of viscosity is of common use in the study of highly non–homologous flows (e.g. Tsharnuter & Winkler 1979; Cioffi, McKee & Bertschinger 1988).

Compared to the above NS solution, the single manipulation in the PV method concerns the viscosity coefficient η, which is used in the simulation. Since the actual particle mean free–path $\bar{l}$ is replaced by the

local cell size, Δx, the viscosity coefficient is increased by the factor $\Delta x/\bar{l}$. Note that the radial component of the stress (eq. [4]) can be either positive or negative, which represents respectively a "tension" or a "pressure". Since shocks lead always to compression, viscous forces act as a pressure. Artificial viscosity should then operate only when the velocity field obeys the conditions

$$3\frac{\partial u}{\partial r} < \boldsymbol{\nabla}\cdot\boldsymbol{u} < 0 \tag{7}$$

This completes the prescription that we use to handle shock waves and to avoid spurious viscous effects.

2.2. Pure Gas Adiabatic Collapse

Let us consider first an adiabatic gas collapse ($\Omega_0 = \Omega_B = 1$). Note that our results, obtained here in an Einstein–de Sitter universe, are also valid for different models, provided that the appropriate change of the cosmic time are made. We show analytically and we confirm numerically that a high density core forms, where no shock dissipation has occurred, surrounded by a self-similar hydrostatic halo, where shock dissipation is very strong.

2.2.1. Initial Conditions

We start at an early epoch t_i, into the linear regime. At that time, every spherical shell has an initial radius r_i. We assume that the velocity field is unperturbed, relative to the homogeneous expansion $v_i = H(t_i)r_i$, and that the initial density contrast has the form

$$\rho_i = \bar{\rho}_i\left(1 + \delta_0\frac{\sin q}{q}\right) \tag{8}$$

This density perturbation does not correspond to a pure growing mode. As long as the initial time is choosen early enough, the decaying mode vanishes quickly. The Lagrangian coordinate of each spherical shell is defined as $q = \Phi_S r_i/R_S$ where $\tan\Phi_S = \Phi_S$ ($\Phi_S \simeq 1.43\pi$). The total mass of the system ($M = 4/3\pi\bar{\rho}_i R_S^3$) is then unperturbed. The collapse epoch of the system is defined as the first shell-crossing time, which writes for these initial conditions

$$t_c = \frac{3\pi}{4}\frac{1+\delta_0}{\delta_0^{3/2}}t_i \tag{9}$$

The two independent parameters which fix then the history of the system are the total mass M and the collapse epoch t_c. The initial *uniform* temperature of the gas is given by the cosmic radiation background, which is tightly coupled to matter from the recombination epoch at $z = 1000$ up to $z = 200$. This leads for $z_i \leq 200$ (see e.g. Anninos & Norman 1994)

$$T_i = 546\left(\frac{1+z_i}{201}\right)^2 \ \mathrm{K} \tag{10}$$

In Section 4, we allow for much higher temperature due to possible reionization processes by stars or quasars UV background radiation fields.

2.2.2. Core Formation

As long as the pressure gradient term remains small compared to the gravitational term (eq. [6]), the pressureless solution of spherical collapse can be used. This regime is valid until $t \simeq t_c$. At that time, it is possible to derive *precollapse* analytical solutions (Moutarde *et al.* 1995). With the notations we use in this paper, this leads to the density profile

$$\rho(q,t_c) = \frac{4}{7}\left(\frac{20}{3}\right)^2 \bar{\rho}(t_c) q^{-4} \tag{11}$$

This behavior is obtained for each initial density profile for which $\partial\rho_i/\partial r = 0$ and $\partial^2\rho_i/\partial r^2 \neq 0$ at $r_i = 0$. Note that such a power law is valid for $q \ll 1$ and $t \simeq t_c$. A useful result is the position of the Lagrangian fluid element q at $t \simeq t_c$.

$$r(q,t_c) = \left(\frac{9\pi}{5}\right)^{\frac{2}{3}} \frac{R_S}{4\Phi_S\delta_0} q^{\frac{7}{3}} \tag{12}$$

One therefore deduces the precollapse density profile $\rho \propto r^{-12/7}$. During this pressureless infall, each fluid element is adiabatically heated to a temperature given by

$$T(q,t) = T_i \left[\frac{\rho(q,t)}{\bar{\rho}(t_i)}\right]^{\frac{2}{3}} \tag{13}$$

which allows us to compute the local sound speed for each fluid element $c_s(q,t_c) \propto T(q,t_c)^{1/2}$. As the velocity field of each infalling fluid element is

$$u(q,t_c) = -\left(\frac{9\pi}{5}\right)^{-\frac{1}{3}} \frac{R_S}{4\Phi_S\delta_0} \frac{\pi}{2t_c} q^{\frac{1}{3}} \tag{14}$$

we can deduce the Mach number of each fluid element defined as $\mathcal{M}(q,t_c) = -u/c_s$.

$$\mathcal{M}(q,t_c) = \left(\frac{5\pi}{7}\right)^{-\frac{1}{3}} \frac{R_S}{4\Phi_S\delta_0} \frac{2\pi}{t_c\bar{c}_s(t_c)} q^{\frac{5}{3}} \tag{15}$$

The fluid element for which $\mathcal{M}(q,t_c) = 1$ reaches its *sonic radius* at $t \simeq t_c$. Its coordinate is of primary importance in our discussion. Let us call the region enclosed by this particular shell the *core* of the forming cluster. For the fluid elements with $q < q_{core}$, the flow is always subsonic, and no shock dissipation occurs in this region. The flow leads to an hydrostatic configuration with nearly uniform density, pressure and temperature.

Outside the core, the flow is supersonic, with higher and higher Mach number for increasing radii. When shocks are strong enough, we enter another regime of the flow leading to a self-similar structure we

identify as the *halo*. Its features are discussed in the next section. Between the core and the halo, there is an intermediate region where shocks are weak and heating is a mixture of adiabatic compression and shock dissipation. This ensures the transition between the adiabatic regime (core), and the strong shock regime (halo). Because the core is in hydrostatic equilibrium, its features remain remarkably stable up to $z = 0$.

It is possible to derive analytically within this adiabatic model the core density, temperature and radius. Using equation (15), we deduce the value of q_{core}. We then obtain with equation (12) the core radius of the cluster

$$r_{core} \simeq 7 \times 10^{-4} \text{ kpc} \left(\frac{1+z_c}{3}\right)^{-\frac{17}{10}} \left(\frac{M}{10^{16}\ M_\odot}\right)^{-\frac{2}{15}} \left(\frac{T_0}{0.014 \text{ K}}\right)^{\frac{7}{10}} \tag{16}$$

T_0 is the average temperature of the unperturbed background at collapse epoch, adiabatically extrapolated until today. M is the cluster mass and z_c the collapse redshift. Note that the core radius is very sensitive to the temperature. The core entropy is indeed equal to the mean background entropy. Its size is directly related to the chosen value of the initial entropy. Because the average baryon density in a purely baryonic universe is fixed by the cosmological parameters, this means that the core radius is mainly determined by the value of the temperature just prior to the collapse. The final density inside the core can be computed using equation (11)

$$n_{core} \simeq 7 \times 10^{7} \text{cm}^{-3} \left(\frac{1+z_c}{3}\right)^{\frac{21}{5}} \left(\frac{M}{10^{16}\ M_\odot}\right)^{\frac{4}{5}} \left(\frac{T_0}{0.014 \text{ K}}\right)^{-\frac{6}{5}} \tag{17}$$

This core density depends strongly on the collapse epoch, because of the $(1+z)^3$ dependence of the mean background density. The core temperature is simply derived using equation (13)

$$T_{core} \simeq 8 \times 10^{6} \text{K} \left(\frac{1+z_c}{3}\right)^{\frac{14}{5}} \left(\frac{M}{10^{16}\ M_\odot}\right)^{\frac{8}{15}} \left(\frac{T_0}{0.014 \text{ K}}\right)^{\frac{1}{5}} \tag{18}$$

These scaling laws agree quite well with the numerical resolution of the hydrodynamics equations, as we will see below.

2.2.3. Halo Formation

As soon as the core has been formed, Lagrangian fluid elements fall towards the center with supersonic velocity, leading to strong shock heating. Let us suppose that a given fluid element is shocked at an epoch given by its own collapse time, in the limit $q \ll 1$, this gives

$$t_s(q) = t_c \left(1 + \frac{3}{20} q^2\right) \tag{19}$$

from which the Lagrangian coordinate of the shock front, at any time after the collapse, is obtained as

$$q_s(t) = 2 \left(\frac{5}{3}\right)^{1/2} \left(\frac{t}{t_c} - 1\right)^{1/2} \tag{20}$$

Using equation (12), we obtain the time dependence for the shock radius, which scales as $r_s \propto (t - t_c)^{7/6}$. As soon as the shock wave is strong enough ($\mathcal{M} \gg 1$), it is possible to estimate the postshock temperature T_2 and density n_2 using Hugoniot-Rankine relations. If we assume that the preshock temperature T_1 is negligible (this is true by definition for a strong shock) and that the postshock velocity u_2 vanishes (hydrostatic flow), this leads to the results

$$kT_2 = \frac{1}{3}\mu m_H u^2(q_s, t_c) \quad \text{and} \quad n_2 = 4\frac{\rho(q_s, t_c)}{\mu m_H} \tag{21}$$

After the shock front, because $u_2(q) = 0$, density and temperature remain constant in time. This implies that the density profile after shock dissipation has the same slope as the precollapse density profile $\rho \propto r^{-12/7}$ (in section 3, we will see that for dark matter the picture is somewhat different) and that the temperature profile scales as $T \propto r^{2/7}$, slowly increasing with radius. As the accretion shock escapes towards the outer part of the cluster, the small q approximation breaks down and the halo features are much more complex.

The basic approximation we make here is the assumption of an hydrostatic postshock flow. When we computed the core properties, we have also neglected all pressure effects which can modify the trajectories. These points have to be tested with numerical calculations which allow us to solve precisely the hydrodynamics equations.

2.3. Numerical Calculations

To test all the formulae presented in the upper sections, and also to illustrate the importance of the numerical prescription used in this paper to treat shocks, we run a simulation with the same initial conditions as previously stated. The run parameters in this section are

$$M = 10^{16}\ M_\odot \quad z_c = 2 \quad T_0 = 0.014\ \mathrm{K} \quad \Omega_B = 1 \tag{22}$$

We start the simulation at $z_i = 200$ and reach $z = 0$ with approximately 10^5 time steps. We plot in Figure 1 density, temperature, velocity and entropy profiles obtained at different redshifts, using equation (5) for the viscous dissipation term. The density and temperature jumps at the shock front are just what is predicted by the Hugoniot-Rankine relations. The assumption of hydrostatic postshock flow appears to be valid with great accuracy, since the postshock velocity field is zero everywhere, and the density and temperature profiles remains constant in time. Note that no spurious oscillations appears in the post shock velocity field. The power laws for the density and the temperature profiles in the halo are in perfect agreement with the analytical derivation. By the virtue of the prescription for viscosity (eq. [5]), the core remains strictly isentropic during the collapse (see fig. [1]). Any other prescription would have led to a spurious core heating, making impossible any description of the most inner part of the cluster.

More interesting is the good agreement between the computed values of the density and the temperature of the core and the predicted values. The computed core density and temperature are respectively $5 \times 10^7 \mathrm{cm}^{-3}$ and $6 \times 10^6 \mathrm{K}$, while the predicted ones were $7 \times 10^7 \mathrm{cm}^{-3}$ and $8 \times 10^6 \mathrm{K}$. The computed core radius is about 2×10^{-3} kpc while the predicted core radius was 7×10^{-4} kpc. The difference is larger for the core radius, since pressure gradients, which have been neglected in our analytical approach, slow down infalling shells slightly before collapse. The important quantity here is the core

entropy, determined quite accurately by both the analytical and the numerical calculations. Note that the very small size of the core ($\sim$ 1 pc) has no influence on the large scale properties of the flow.

When the entropy profile starts to rise, we enter the halo regime, where strong shock dissipation takes place. When the shock front reaches outer regions of the cluster, the density profile get sharper, since the small q approximation is not valid anymore. The density profile slopes from a $r^{-12/7}$ law in the center to a r^{-3} law in the outer parts.

3. A FLUID MODEL FOR DARK MATTER

The collisionless component of the universe is supposed to dominate the total gravitational potential at nearly all scales. In a high dynamical range simulation, the main difficulty is to get for dark matter a resolution comparable to that achieved for the gas component, ranging up to 10 orders of magnitude in density.

We first approach the problem of dark matter dynamics by the traditional "spherical shells model" (Hoffman, Olson & Salpeter 1980; Peebles 1982; Hoffman, Salpeter & Wasserman 1983; Hausman, Olson & Roth 1983; Martel & Wasserman 1990; Thoul & Weinberg 1995). In this description, the collisionless particles are distributed over N concentric shells of individual masses m and radius r. As long as the mass M included below a given shell is constant, its dynamics is determined by Kepler's laws for a central potential motion. The highest accuracy on kinematics and energy conservation ($\sim 10^{-15}$ for a SUN station) is achieved by using this exact solution for each shell, up to shell crossing. At that time, new total energies can be calculated, and new exact trajectories are computed, until the next shell crossing time, and so on. This time–consuming procedure guarantees in principle a very high level of accuracy, since trajectories are analytically treated. However, in the limit of a continuous dark matter distribution with zero angular momentum, shell crossings occur continuously at the center of the spherical distribution, where the density is infinite. With a finite shell number, the first crossings (in radii) occur in a rapidly shrinking region, the size of which ultimately excludes any numerical solution. Moreover, a correct sampling of the shell distribution in the inner regions (in particular over the size of the adiabatic core of the gas) requires an excessive number of shells, resulting in a definitely prohibitive computing time.

We have also examined various adaptations of the Particle Mesh (PM) technics, abandoning the quality of the semi-analytical solution. Again, the very small inner scales were not well-sampled, mainly because of the Eulerian nature of PM schemes.

We propose in the following a fluid treatment for dark matter, which reproduces properly some aspects of the self-similar solutions of dark matter collapse, derived in particular by Fillmore and Goldreich (1984) (hereafter FG) and Bertschinger (1985). This unusual choice, initially dictated by the high resolution requirements of Lagrangian simulations, provides a new insight on collisionless dark matter dynamics. Moreover, it prevents for any two–body relaxation effect, inherent to any description of dark matter with a finite number of shells.

3.1. Dark Matter in Spherical Geometry

The collisionless dark matter fluid is described by the velocity distribution function $f(\boldsymbol{r}, \boldsymbol{v}, t)$, which evolves according to the Poisson–Vlasov equation. For a spherical system of particles moving along radial

orbits, it reduces to $f(r, v_r, t)$, where v_r is the individual particle radial velocity. The hydrodynamical, bulk velocity of the fluid is $u =< v_r >$.

In a collapsing halo, three different regions can be distinguished:

- The single stream, infall region, where the motion is purely Keplerian. The distribution function reduces to a δ function, centered on the local flow velocity.
- The relaxed core, where the dark matter fluid has been heated up by phase mixing. We show in a companion paper (Teyssier, Chièze & Alimi 1997) that, for the wide class of self–similar collapse, the adiabatic invariance of the gravitational potential ensures in this region the evenness of the distribution function in velocity space. We take advantage of this property to derive the equation of state of the dark matter fluid.
- The relaxation region, between the single stream and the relaxed regions, where the velocity distribution can only be described by solving the Poisson–Vlasov equation. We assume here that this dissipation region is of finite size, so that one can connect the flow properties on both sides, by the mass, momentum and energy conservation laws. The resulting "jump" conditions are the analogous of the Hugoniot–Rankine relations for classical fluids. Therefore, the preceding discussion of dissipation in fluids can be extended to dark matter.

3.2. Dark Matter Fluid Thermodynamics

We first derive the equation of state of dark matter, in the relaxed region where our fluid approach is valid, from virial and from thermodynamical considerations (see also Teyssier, Chièze & Alimi 1997 for further comments).

We consider a large system of particles, with an equilibrium spherical distribution. Particles are moving only along radial paths, as required by the spherical dark matter model. Consider the N particles interior to the sphere (Σ) of radius L and mass M. The aforementioned evenness of the distribution function is equivalent to assume a quasi–stationary state, with no mass and energy flux through any surface element. An equal number of particles are flowing in and out the system, crossing (Σ) with opposite velocities. These two opposite flows result in a net momentum flux, $p\boldsymbol{n}dS$, through any surface element drawn on (Σ), with a direction opposite to the normal $\boldsymbol{n}$ to the surface element dS. It is thus without consequence to materialize the surface (Σ) by a reflecting sphere, on which the exterior fluid exerts a uniform, normal force $-p\boldsymbol{n}$ per unit surface. Defining the net force exerted on the surface (Σ) by the fluid exterior to the system by

$$-\bar{\omega} = -\int_{\Sigma} p\ \boldsymbol{n}\cdot\boldsymbol{n}\ dS = -4\pi L^2 p \tag{23}$$

one can see immediately that the total kinetic energy of the system, E, obeys the virial equation

$$2E = \bar{\omega} L \tag{24}$$

This is the equation of state of the system, which has been derived here from purely mechanical considerations, assuming a even particles distribution function.

The thermodynamical point of view leads to more specific results. The energy E and the entropy s are the state variables of the system. Both are extensive quantities relative to the total number of particles N. Since each particle has only one translational degree of freedom, the entropy, function of N, E and of the external parameter L, has the form

$$s\ (E,L) = Nk\ \left(\ln\frac{L}{N} + \frac{1}{2}\ln\frac{E}{N}\right) + s_0 \tag{25}$$

The first and second principle of thermodynamics lead to the expression

$$dE = Tds - \bar{\omega}dL \tag{26}$$

where one has defined the intensive conjugated variables of S and L :

$$T = \left(\frac{\partial E}{\partial s}\right)_L = 2\ \frac{E}{Nk} \quad \text{and} \quad \bar{\omega} = -\left(\frac{\partial E}{\partial L}\right)_s = 2\ \frac{E}{L} \tag{27}$$

which is again the equation of state of the fluid. Clearly, for an isentropic evolution, one has

$$\left(\frac{\partial \bar{\omega}}{\partial \mu}\right)_s = 3\ \frac{\bar{\omega}}{\mu} \tag{28}$$

where we have defined the *linear* mass density $\mu \equiv \partial M/\partial L$. It can be easily shown that $(\partial\bar{\omega}/\partial\mu)_S$ is just the square of the sound velocity. Specific heats are properly defined for transformations respectively at constant $\bar{\omega}$ and constant L. From equations (24) and (25) one readily obtain the corresponding specific heats $C_{\bar{\omega}}$ and C_L as

$$C_{\bar{\omega}} = \frac{3}{2}Nk \qquad C_L = \frac{1}{2}Nk \tag{29}$$

With this peculiar understanding of the specific heats, this monodimensional gas can be considered as a $\gamma^{(1)} \equiv C_{\bar{\omega}}/C_L = 3$ gas. The thermodynamical equilibrium of a (gravitational) force free system is characterized by the uniformity of T, $\bar{\omega}$ which imply a uniform *linear* mass density μ. In other words, the equilibrium mass density ρ and particle velocity dispersion σ profiles are

$$\rho \propto L^{-2} \qquad \sigma = Const. \tag{30}$$

However, starting from an arbitrary distribution of particles in phase space, thermodynamical equilibrium can only be reached through gravitational interactions, since particles are supposed to be collisionless.

3.3. Dark Matter Fluid Equation of Motion and Dissipation

In the dark matter spherical model, where particles have no angular momentum, no initial velocity dispersion, and suffer no collision, their orbits of zero eccentricity degenerate into purely radial trajectories. The motion of an individual particle is thus monodimensional, contrary to a classical gas for which collisions

populates the three translational degrees of freedom. Defining the hydrodynamical velocity $\boldsymbol{u}$ as the mean local velocity of particles, and the gravitational potential as $\Phi(r,t)$, the equation governing adiabatic fluid motions is immediately derived from the definition of $\bar{\omega}$

$$\frac{du}{dt} = -\frac{1}{\mu}\frac{\partial \bar{\omega}}{\partial r} - \frac{\partial \Phi}{\partial r} \tag{31}$$

which express the conservation of the momentum of a spherical shell of unit mass. The position coordinate is now written as usual in spherical geometry r. The equation of motion (eq. [31]) is hyperbolic and thus leads to the formation of shocks. It cannot account for the phase mixing, which results, according to the Vlasov–Poisson approach, from shell crossings. As already stated, we assume that the relaxation region, identified as the first leading caustics in the solutions of the Vlasov equation, is of finite size. The upstream and downstream flow properties are connected by the continuity of the mass, momentum and energy flows, which write

$$\mu_2 u_2 = \mu_1 u_1 \tag{32}$$

$$\bar{\omega}_2 + \mu_2 u_2^2 = \bar{\omega}_1 + \mu_1 u_1^2 \tag{33}$$

$$\left(\frac{3}{2}\bar{\omega}_2 + \frac{1}{2}\mu_2 u_2^2\right) u_2 = \left(\frac{3}{2}\bar{\omega}_1 + \frac{1}{2}\mu_1 u_1^2\right) u_1 \tag{34}$$

where the subscripts refer to the upstream and downstream regions. Consequently, the "jump" conditions, which must be verified across the relaxation region, are

$$\mu_2 = 2\mu_1 \quad u_2 = \frac{1}{2}u_1 \quad \bar{\omega}_2 = \frac{1}{2}\mu_1 u_1^2 \tag{35}$$

Since they do not depend on the detailed relaxation processes, they are also the solutions, for our dark matter fluid, of the analogous of the Navier–Stokes equations (which however do not provide the exact solution *inside* the relaxation layer). Due to the symmetry of the system, the viscous forces acting on a fluid element is purely radial, so that the equivalent of the Navier–Stokes equation is

$$\frac{du}{dt} = -\frac{\partial}{\partial M}(\bar{\omega} + \bar{\bar{\omega}}) - \frac{\partial \Phi}{\partial r} \tag{36}$$

where $\bar{\bar{\omega}}$ is the viscous force defined on the surface of the sphere of radius r. We determine now the rate at which energy is dissipated in a fluid element of unit mass. The variation of its kinetic energy, K, can be written as

$$\frac{dK}{dt} = -\frac{\partial(\bar{\omega}u)}{\partial M} - \frac{\partial(\bar{\bar{\omega}}u)}{\partial M} - u\frac{\partial \Phi}{\partial r} + \bar{\omega}\frac{\partial u}{\partial M} + \bar{\bar{\omega}}\frac{\partial u}{\partial M} \tag{37}$$

The first, second and third terms of the rhs represent respectively the rates at which the pressure, viscous and gravitational forces do work on the fluid element. This total amount of energy is not entirely restored as flow kinetic energy. Indeed, the two last terms represent the energy which goes into heat, the first of which is the compression work. Therefore, the expression

$$\dot{q} = -\bar{\bar{\omega}} \frac{\partial u}{\partial M} \tag{38}$$

represents the rate of increase of the internal energy resulting from the dissipation of the kinetic energy by viscosity. Since dissipation can only result in an entropy increase, one has furthermore

$$\bar{\bar{\omega}} \frac{\partial u}{\partial M} < 0 \tag{39}$$

The expression of $\bar{\bar{\omega}}$ must be definite and positive in dissipative regions, that is in shell crossing regions, near the leading caustic, and zero elsewhere. In this monodimensional (radial) fluid, there is no distinction between the rate of strain and the rate of increase of the length of a linear element of fluid, $\partial u/\partial r$. For these reasons, the dissipative force can be written as

$$\bar{\bar{\omega}} = -\bar{\eta} \frac{\partial u}{\partial r} \tag{40}$$

which automatically verifies the irreversibility condition expressed by equation (39), provided that $\bar{\eta} > 0$. This expression of the viscous force would be in principle valid for a collisional monodimensional fluid, for which the particle velocity distribution is governed by collisions. This is not true for collisionless material, where the particle velocity distribution remains completely determined by the initial conditions until the occurrence of the first shell crossing. Until that stage, the collisionless fluid conserves the memory of the initial velocity distribution, contrary to a collisional gas for which this memory is abolished after a few collision times. In our fluid description, it is reasonable to consider that shell crossing, and thus phase mixing, actually occurs when the criterion

$$\frac{\partial u}{\partial r} - \frac{u}{r} < 0 \tag{41}$$

is fulfilled. We shall see in the following section that, according to this criterion, the position of the fluid relaxation layer (that is, the shock position) coincides quite accurately with the position of the leading caustic of collisionless material.

3.4. Self Similarity Solutions for Dark Matter

The role which is essentially assigned to dark matter is to provide the gravitational potential well in which gas eventually condenses. Therefore, two main requirements must be fulfilled by a fluid treatment. At first, the over–all dark matter mass profile must be correctly described. Second, the time dependence of the growth of the relaxation region must be also correct. We check here these two points by comparing our fluid model results to some known self–similar solutions of the problem of dark matter collapse.

Similarity solutions have been found by FG for the problem of the collapse of cold, collisionless matter in a perturbed Einstein–de Sitter universe. The scale–free initial mass perturbation they have considered is of the form

$$\frac{\delta M}{M} = \left(\frac{M}{M_0} \right)^{-\epsilon} \tag{42}$$

where M_0 is a scaling mass and $0 < \epsilon \leq 1$. The initial velocity field they have considered is unperturbed relative to the Hubble flow. After shell crossing, the dark matter density profiles they obtained are well fitted by a power law $\rho(r) \propto r^n$ at small radii, with, for spherical geometry, the following values for n

$$n = -2 \text{ for } \epsilon \leq \frac{2}{3} \quad \text{and} \quad n = -\frac{9\epsilon}{3\epsilon + 1} \text{ for } \epsilon \geq \frac{2}{3} \tag{43}$$

We present in Figure (2) the overdensity profiles obtained at different redshifts for the cases $\epsilon = 0.2$, 0.5, 0.8 and 1. The radius have been rescaled at each epoch to the self–similar radius defined as $\lambda = r/r_{ta}$ where r_{ta} is the current turn–around radius. Except naturally the caustics, the overdensity profiles we obtain are exactly those presented in FG. In our fluid model, dissipation occurs for dark matter through shock waves. The position of the shock front marks the first shell crossing, and therefore has to be close to the first caustic. We define the shock front as the point where the second derivative of the velocity field reaches its minimum. We plot the position of this shock front in Figure (2) as an arrow on the λ axis. Note that both the power law and the position of the first caustic are in very good agreement between our fluid model and the collisionless self–similar solutions. Note also that the dynamical range in radius we obtained is much larger than in any other dark matter simulations, allowing us to achieve very high resolutions.

The case $\epsilon = 1$ corresponds to the secondary infall onto an initially overdense perturbation embedded in an Einstein–de Sitter universe. Bertschinger (1985) has examined this situation in details, both for collisionless and collisional fluids. Our result is quantitatively similar to the relevant collisionless overdensity profiles presented in Table 4 of Bertschinger (1985). This author found that the position of the leading caustic for dark matter is $\lambda = 0.364$. We recover this value with 2% accuracy within our fluid model. Bertschinger (1985) found that the shock front position for a $\gamma = 5/3$ gas was $\lambda = 0.339$, very close to the dark matter leading caustic. He noticed however that $\gamma = 3$, pertinent to a one dimensional gas, should have been preferred, although he obtained in that case $\lambda = 0.600$. This apparent paradox has been elucidated here (section 3.2).

3.5. Arbitrary Initial Conditions

The similarity solutions for dark matter collapse are well recovered within our fluid model. It reproduces also the precollapse scale invariance obtained by Moutarde et al. (1995) for a wide range of initial density profile. This precollapse scale invariance allows to built up naturally the conditions for self–similar collapse, for which our fluid model is fully valid. As a matter of fact, we plot in Figure (3) the evolution of the density profile for a pure dark matter collapse, using the same initial conditions as in section 2. Before the first caustic, the density profile follows the precollapse scale invariance $\rho \propto r^{-12/7}$, and after shell crossings, the density is well fitted by the power law $\rho \propto r^{-2}$. It is important to notice that the mass distribution is not the same than for the pure gas collapse. Moreover, the postshock velocity vanishes exactly for the gas, leading to a constant central density, while for dark matter, the central density increases continuously with time, following the time scaling law given by FG for the case $\epsilon = 4/9$, which corresponds to a precollapse density profile with a slope $n = 12/7$. At late epoch, and for large radii, the self–similar regime is no longer valid, and a fully numerical treatment is necessary.

4. COUPLED DARK MATTER AND GAS EVOLUTION

In section 2, we derived the evolution of a pure gas initial perturbation, while in section 3, we derived the evolution of a pure dark matter one, using for both case the same initial profile. We conclude that these two cases give different results for the mass distribution within the cluster ($\rho \propto r^{-12/7}$ for gas and $\rho \propto r^{-2}$ for dark matter). In this section, the fluid we consider is a mixture of gas and dark matter particles. This leads to a new important parameter for the dynamics of the forming cluster, the gas fraction of the unperturbed background Ω_B (we still assume an Einstein–de Sitter universe with $h = 0.5$, but our results are valid for any cosmological parameters).

4.1. Halo Structure

For a dark matter dominated universe (with $\Omega_B \ll 1$), it seems natural to obtain for the gas density profile very similar results than for dark matter. To test this hypothesis, we run three simulations with the same initial parameters

$$M = 10^{16}\ M_\odot \quad z_c = 2 \quad T_0 = 0.014\ \mathrm{K} \tag{44}$$

allowing the baryon density parameter to take three different values

$$\Omega_B = 0.01 \quad \Omega_B = 0.9 \quad \Omega_B = 0.99 \tag{45}$$

We choose a low initial temperature, which, as we know from section 2, leads to a very small core ($r_{core} \simeq 10^{-3}$ kpc). This is of course very far from the observed values in large X-ray clusters where $r_{core} \simeq 100$ kpc. We are interested here in the halo structure, where a power law is observed for both dark matter and gas density profiles. The core problem will be addressed below.

We plot in Figure (4) the gas and dark matter overdensity profiles obtained at z = 0 for various Ω_B. For sake of comparison, we also plot the gas density profile for the $\Omega_B = 1$ case, and the dark matter density profile for the $\Omega_B = 0$ case. Note that, even for low values of the baryon density parameter, the gas distribution does not follow the dark matter distribution. The gas density profile is steeper than for the pure gas case, but does not fit the dark matter profile. This is due to the presence of a core that prevents gas to fall deeper in the dark matter potential well, and to the shock relations followed by gas (three internal degrees of freedom) which differ from those followed by dark matter (one internal degree of freedom). Note also that the dark matter density profile is insensitive to the value of Ω_B. The main effect of dark matter on the gas distribution is to compress the core and the halo after the collapse epoch. This leads to a strong heating of the core due to adiabatic compression only. The resulting temperature is much higher than for the pure gas case. The slope in the temperature profile changes also slightly, leading to a much more isothermal profile. For $\Omega_B \simeq 1$, the gas distribution recovers the same characteristics than for the pure gas case.

One interesting quantity is the gas fraction, defined as $f_{gas} = M_{gas}(\leq r)/M_{tot}(\leq r)$, the ratio of the enclosed gas mass to the total gravitational mass. Because the slope of the dark matter density profile is steeper ($\rho_{dark} \propto r^{-2}$) than for gas ($\rho_{gas} \propto r^{-12/7}$), the gas fraction increase with radius. In the core, f_{gas} has a very low value, because dark matter dominates. In the halo, for a dark matter dominated Universe,

f_{gas} increases continuously with radius as $r^{2/7}$, with $f_{gas} \simeq \Omega_B$ in the most outer regions. We plot in Figure (4) f_{gas} versus the total mass as in DJF (see their fig. [5]). When we compare our profile with the observed ones in the most massive clusters, we find an excellent agreement.

4.2. The Core Problem

We saw in section 2 that, for very general initial conditions, a core forms with very high density, and we just saw in this section that if dark matter is present, the central density is even higher. The observed core density in massive X–ray clusters is not higher than 10^{-1} cm^{-3}, with core radii of the order of a few hundred kpc. This apparent discrepancy is due to the fact that in adiabatic models the initial entropy of the primordial gas is very low, leading to very small cores. We saw that within adiabatic models, it was impossible to generate entropy inside the core, even within a dark matter dominated scenario. When cooling is taken into account, the situation is worst: the resulting decrease in entropy naturally leads to the formation of an ultra high density central core, in about a free–fall time. It seems clear that this uncomfortable situation is unavoidable, if one restrict to dynamical considerations only. On the other hand, it is possible to imagine many entropy generating processes, such as supernovae driven winds, UV background radiation field, ambipolar diffusion, electronic conduction and so on. It is far beyond the scope of this paper to treat all this processes. To see an interesting review of this question, see Sarazin (1990). We simplify greatly the problem by considering a simple model, that we describe now.

We consider an homogeneous heating process, such as a background UV radiation field generated by primordial quasars or stars. We model this process by turning on gas heating at say z = 5, and by imposing the following conditions. If $T < 10^4$ in a cell, we reset the gas temperature by imposing $T = 10^4$. On the contrary, if $T \geq 10^4$, the gas temperature in the cell remains unchanged. This is a continuous entropy generating process, which has also physical support from the processes we just enumerated. In this framework, the background temperature is a free parameter, and we consider here 3 different values

$$T_{bg} = 10^4 \text{ K} \quad T_{bg} = 10^5 \text{ K} \quad T_{bg} = 10^6 \text{ K} \tag{46}$$

The last value is much higher than the permitted temperature obtained by quasars spectra, but it gives us a limit for high entropy generating processes, such as supernovae driven winds. We take the following parameters for these three runs

$$M = 10^{16}\ M_\odot \quad z_c = 2 \quad \Omega_B = 0.1 \tag{47}$$

This method enables us to use the analytical formulae derived in section 2 for the pure gas collapse, using $T_0 = T_{bg}(1 + z_c)^{-2}$.

We plot in Figure (5) the resulting structure we obtained at z = 0. Note that the core density is much lower than for the other cases. The core entropy has been greatly enhanced, leading, as expected, to a more extended core. Outside the core, the profiles remain unchanged by the heating process relative to the purely adiabatic case. Note also that we predict with our analytical model a decrease of the central density by a factor of 16 between the three runs, which is exactly what we recover in Figure (5). The dark matter overdensity profile is still insensitive to the gas distribution, as noticed in the last section.

Note that even for the higher temperature run, the core size is still unrealistic. This is partly due to

the large mass and collapse redshift we use in our simulations. We believe however that in real clusters the initial entropy level should be as high as $T_{bg} \simeq 10^7$ K, in order to obtain large enough core radii. An interesting study, that we postpone to a next paper, would be to deduce from observed X–ray clusters the required entropy level to explain their core sizes and densities. This could give important clues to seek for efficient heating processes in galaxy clusters.

5. CONCLUSIONS

The main goal of this paper is the study at very high resolution of the collapse of cosmological structures. This requirement implies necessarily a 1D approach. Pancakes formation has been thoroughly studied over the past decade (Zel'dovich 1970; Bond *et al.* 1984; Shapiro & Struck–Marcell 1985; Anninos & Norman 1994), while spherical collapse remained unexplored at an equivalent resolution (in our case, the central resolution is of the order of 0.1 pc).

In the adiabatic case examined in this first paper, the main features of the virialized structures result from the dissipation of supersonic infall motions. One therefore should take care of the method used to handle shock waves, especially in spherical geometry. Within the artificial viscosity method, we derive the form of the viscous forces one should use to get a correct description of shocks, both in time and space. This general prescription can be easily adapted to 3D hydrodynamics.

This provides a clear account of the formation of core–halo structures in the pure gas case. During the collapse, the flow is characterized by a subsonic inner region (the core), surrounded by a large envelop where strong shock dissipation occurs (the halo). The core and the halo are merely the remnants of the adiabatic and dissipative regions of the flow. The size of this isentropic core is therefore mainly determined by the initial entropy of the primordial gas. We obtain for a wide range of initial conditions very small cores with very high density, definitely ruled out by X–ray observations.

These features are not qualitatively affected by the presence of the dark matter component, but quantitatively the situation is even worse. The main effect of dark matter is to compress further the gas core, but with subsonic velocities, so that, again, no entropy is generated.

However, this conclusion relies on the treatment of the inner gravitational field dominated by dark matter. Due to the divergence of the potential at the center, methods using particles are excluded in practice by the current computers limitations. For that reason, we propose a fluid approach describing the dynamics of dark matter. This method successfully reproduces the analytical solutions of the self–similar spherical collapse. However, caustics are smoothed out within this model, but the leading shell crossing appears as a discontinuity in the dark matter flow at the correct location. This model provides moreover a new insight in dark matter spherical dynamics, treated here as a $\gamma = 3$ monodimensional fluid.

We specifically studied initial conditions with a single spherical Fourier mode as initial density perturbation. The results we obtain are then valid for a wide range of arbitrary spherical initial conditions. We show analytically that in the pure gas case the halo has a density profile $\rho \propto r^{-12/7}$, while in the pure dark matter case, it is close to $\rho \propto r^{-2}$. The numerical results are in perfect agreement with this scale invariance. The specific features of the coupled case are the followings. We show that, even for very low Ω_B, the gas never strictly follows the dark matter particles. This is due to their different numbers of translational degrees of freedom. As a consequence, the gas mass fraction is an increasing function of radius. Gas is more smoothly distributed than dark matter, with a density profile in–between those obtained for

pure gas and pure dark matter collapse. Adiabatic models are then an natural explanation of the observed *antibias* in X–ray clusters (DJF). In the most outer regions, the gas mass fraction reaches the unperturbed value Ω_B.

These conclusions can be naturally affected by the actual geometry of a fully 3D gravitational dynamics, in which the collapse occurs in sheet–like structures, in filaments and also in quasi–spherical knots. This could lead to different density profiles, mainly in the inner part where rotational effects are expected to be important. Recent 3D studies show indeed that the mass profile in clusters may be smoother than the singular isothermal sphere in the central part ($\rho \propto r^{-1}$; see Navarro et al. 1995; Cole & Lacey 1996; Tormen, Bouchet & White 1996). However, even in 3D, the dense adiabatic cores are likely to merge subsonically, leaving unsolved the core problem. Anninos & Norman (1996) investigated the influence of the actual numerical resolution on a simulated cluster. They conclude that the gas central density does not converge, even for their highest resolution run. In fact, we show in this paper that the typical size of cores obtained for an adiabatic collapse should be about 10^{-3} kpc. Heating processes are therefore unavoidable to obtain measurable core radii. Antibiasing has been also investigated in 3D simulations (Kang et al. 1994; Martel et al. 1994), where a strong segregation between gas and dark matter has been detected. However, Steinmetz & White (1996) have shown that this effect could be due to a spurious heating of the gas, due to the finite number of particles used in 3D simulations. We stress here that the antibias discussed in this paper, in a rather constrained geometry, has a firm physical origin: the different dimensionality of gas ($\gamma = 5/3$) and dark matter ($\gamma = 3$) phase spaces. This result was obtained using analytical or semi–analytical methods, free from any two–body relaxation or spurious viscous effects.

We briefly investigate in this paper the initial entropy level which would lead to more realistic cores properties. We find that UV radiation fields, accounting only for a background temperature of 10^4 K up to 10^6 K, are unable to solve the core problem. Consequently, it appears that the initial entropy level that could alleviate this short cut is very high, and must result from a background temperature as high as 10^7 K. We therefore analyze in a companion paper the thermodynamical aspects of collapse, regulated by the balance between gas cooling and new energy sources like the feedback from star formation.

We thank an anonymous referee for his careful reading of the manuscript and his constructive comments which have improved the quality of our work.

REFERENCES

Anninos, W.Y., & Norman, M.L., 1994, ApJ, 429, 434

Anninos, P.A., & Norman, M.L., 1996, ApJ, 459, 12

Bertschinger, E., 1985, ApJS, 58, 39

Blottiau, P., Chièze, J.-P. & Bouquet, S., 1988, A&A, 207, 24

de Boisanger, C., Chièze, J.-P. & Meltz, B., 1992, ApJ, 401, 182

Bond, J.R., Centrella, J. Szalay, A.S., & Wilson, J.R., 1984, MNRAS, 210, 515

Briel, U.G., Henry, J.P. & Bohringer, H, 1992, A&A, 259, L31.

Cioffi, McKee & Bertschinger, 1988, ApJ, **334**, 252

Chièze, J.-P., Teyssier, R., & Alimi, J.-M., 1997, in preparation.

Cole, S., Lacey, C.G., 1996, MNRAS, in press.

David, L.P., Jones, C., & Forman, W., 1995, ApJ, 445, 578 (DJF).

Fillmore, J.A., & Goldreich, P., 1984, ApJ, 281, 1 (FG)

Flores, R.A. & Primack, J.R. 1996, ApJ, 457, L5.

Hausman, M.A., Olson, D.W., & Roth, B.D., 1983, ApJ, 270, 351.

Hoffman, G.L., Olson, D.W. & Salpeter, E.E., 1980, ApJ, 242, 861.

Hoffman, G.L., Salpeter, E.E., & Wasserman, I., 1983, ApJ, 268, 527.

Hughes, J.P., 1989, ApJ, 337,21.

Kang, H., Cen, R., Ostriker, J.P., & Ryu, D., 1994, ApJ, 428, 1.

Landau, L.D. & Lifshitz, E.M., 1982 "Course of Theoretical Physics, Volume 6: Fluid Mechanics" (Pergamon Press)

Martel, H., Shapiro, P.R., Valinia, A., & Villumsen, J.V., 1994, in Dark Matter, eds S.S. Holt & C.L. Bennett, AIP Conference Proceeding 336, p.441.

Martel, H., & Wasserman, I., 1990, ApJ, 348, 1.

Mellier, Y., Dantel-Fort, M., Fort, B. & Bonnet, H. 1994, A&A, 289, L15.

Moutarde, F., Alimi, J.-M., Bouchet & F.R., Pellat, 1995, ApJ, 441, 10

Navarro, J.F., White, S.D.M., 1993, MNRAS, 265, 271

Navarro, J.F., Frenk, C.S., White, S.D.M., 1995, MNRAS, 275, 720.

Pearce, F., Thomas, P.A. & Couchman, H.M.P., 1994, MNRAS, 268,953.

Peebles, P.J.E., 1982, ApJ, 257, 438.

Rothenflug, R., Magne, N., Chièze, J.-P., Ballet, J., 1994, A&A, 291, 271

Sarazin, C.L., 1990, "X-ray spectra of Clusters of Galaxies" (Cambridge University Press: Cambridge, England and New York)

Shapiro, P.R., & Struck-Marcell, C., ApJSS, 57, 205

Steinmetz, M., & White, S.D.M., 1996, submitted to MNRAS, astro–ph/9609021

Teyssier, R., Chièze, J.-P., & Alimi, J.-M., 1997, ApJ, in press.

Thoul, A.A., & Weinberg, D.H., 1995, ApJ, 442, 480

Tormen, G., Bouchet, F.R., & White, S.D.M., 1996, MNRAS, submitted.

Tscharnuter, W.-M., & Winkler, K.-H., 1979, Comput. Phys. Comm., 18, 171

Tyson, J.A., Valdes, F. & Wenk, R.A. 1990, ApJ, 349, L1.

Von Neumann, J., & Richtmyer, R.D., 1950, J. Appl. Phys., **21**, 232.

White, S.D.M., Navarro, J.F., Evrard, A.E., & Frenk, C.S. 1993, Nature, 366, 429.

Wu, X.P., & Hammer, F. 1993, MNRAS, 262, 187.

Zel'dovich, Ya. B., 1970, A&A, 5, 84

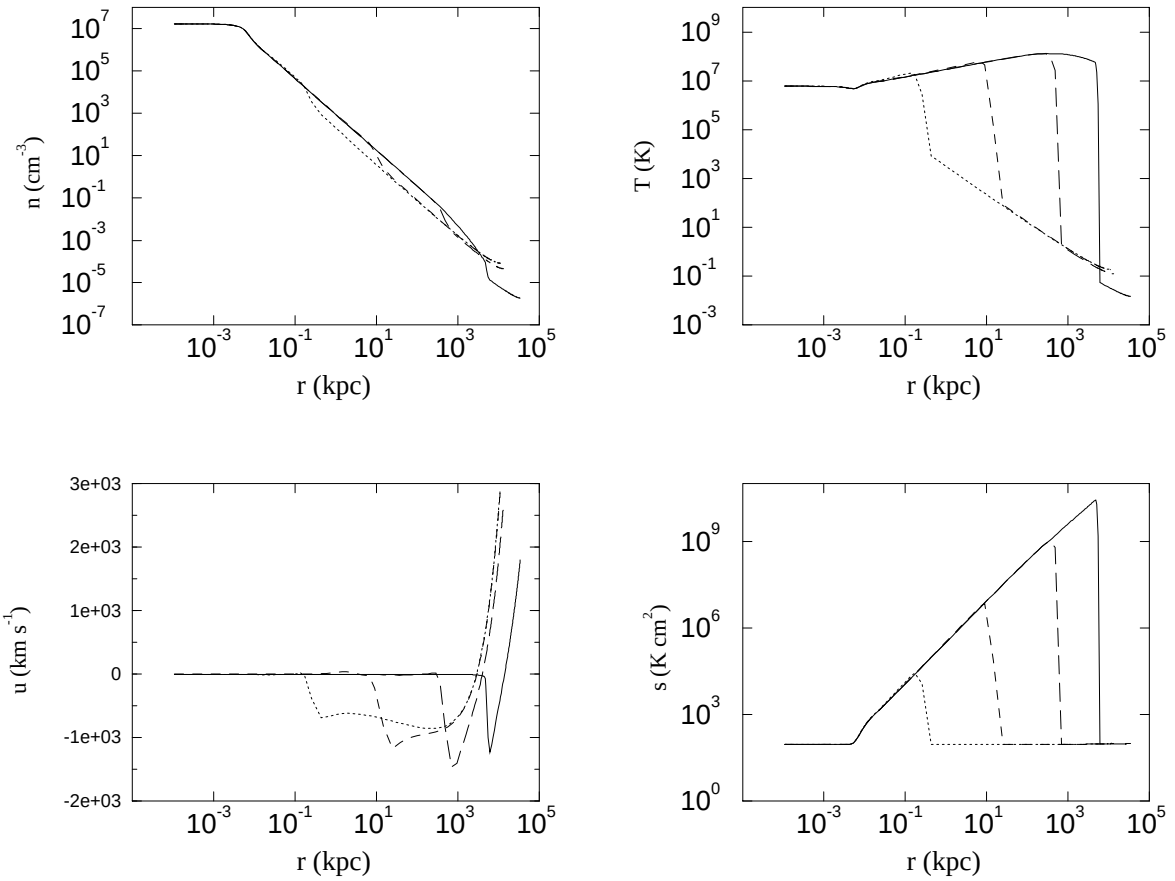

Fig. 1.— Density, temperature, velocity and entropy profiles obtained at z=1.995 (dotted line), 1.98 (dashed line), 1.5 (long-dashed line) and 0 (solid line) for the pure gas collapse with parameters $M = 10^{16}\ M_{\odot}$, $z_c = 2$ and $T_0 = 0.014$ K .

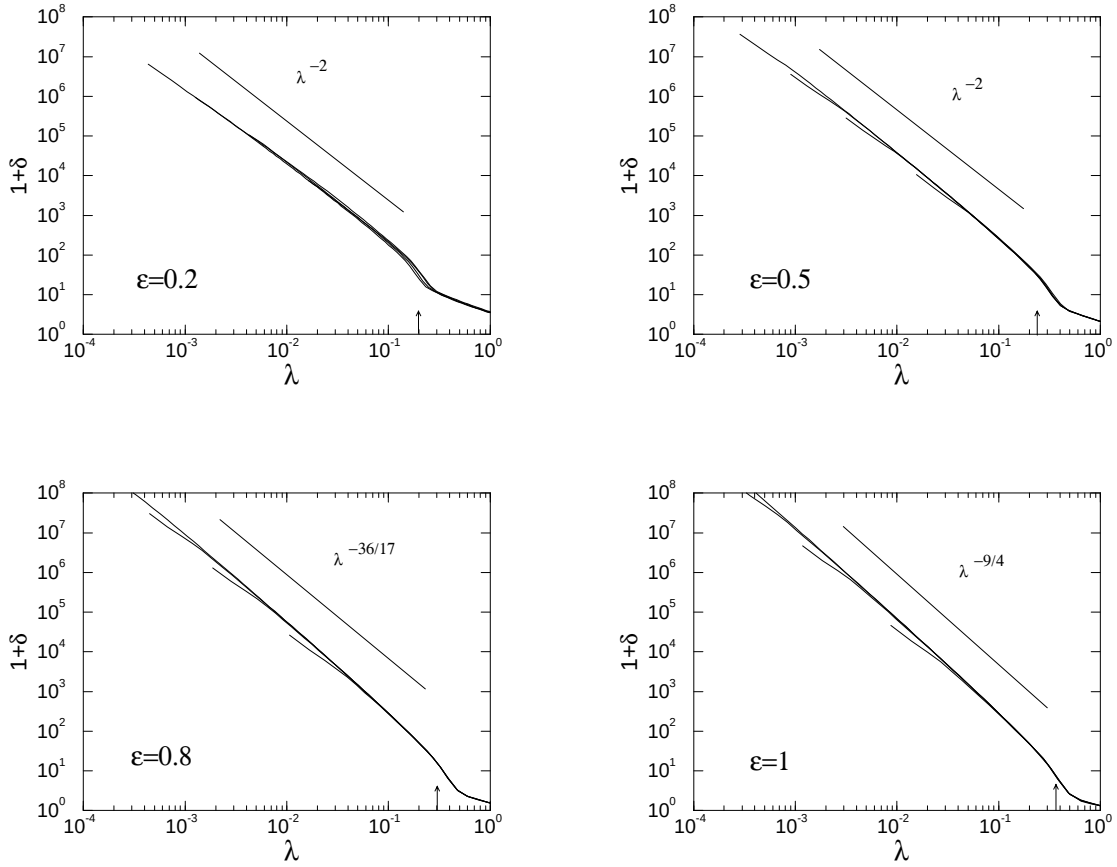

Fig. 2.— Over-density profiles versus the self–similar radius λ (see Section 3.4) obtained at different redshifts for the pure dark matter case. We used scale invariant initial conditions with $\epsilon = 0.2, 0.5, 0.8$ and 1. The self similarity is perfectly recovered, as well as the correct power law. The position of the dark matter "shock front" (arrows) is exactly at the radius of the first caustic calculated by Fillmore & Goldreich (1984).

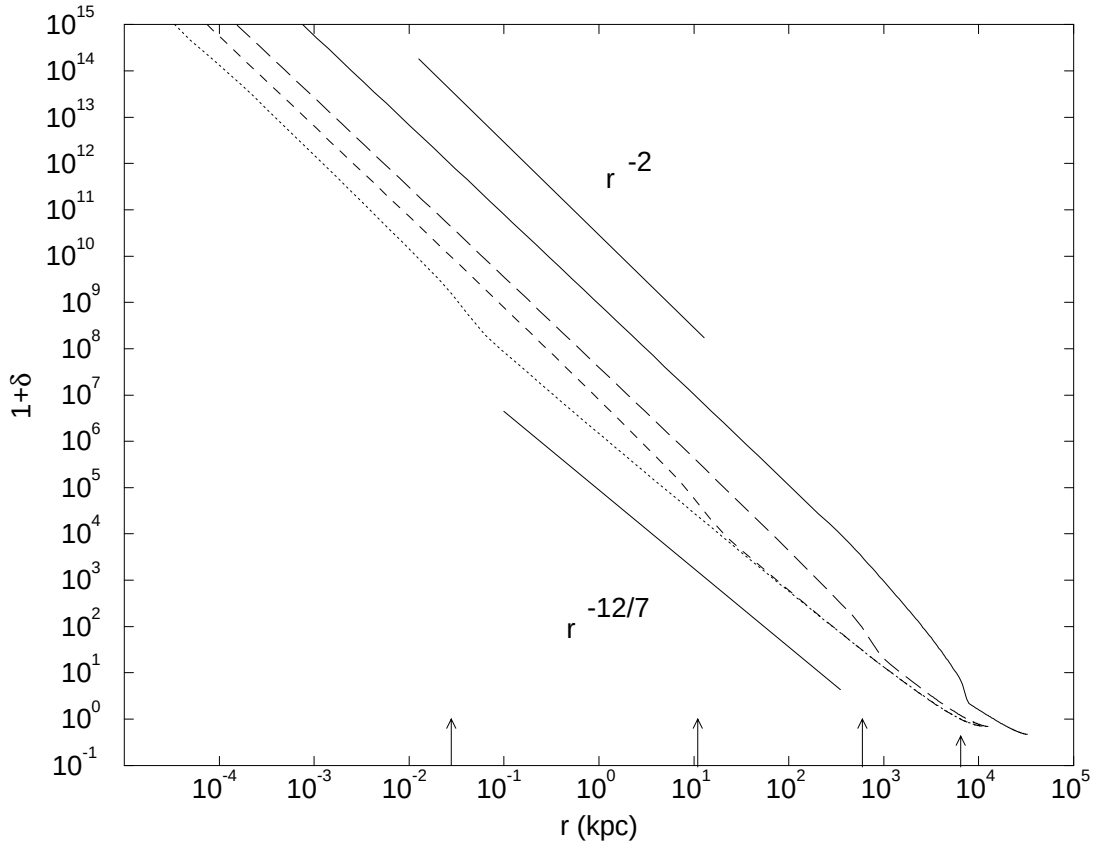

Fig. 3.— Over-density profiles versus radius obtained at redshifts $z = 1.995$ (dotted line), 1.98 (dashed line), 1.5 (long-dashed line) and 0 (solid line) for the pure dark matter case. We used a single Fourier spherical mode as initial perturbation. Before the dark matter "shock front"(arrows), the pre-collapse slope $n = -12/7$ is recovered. After that, the corresponding self similarity solution of Fillmore & Goldreich (1984) is obtained with a slope close to $n = -2$.

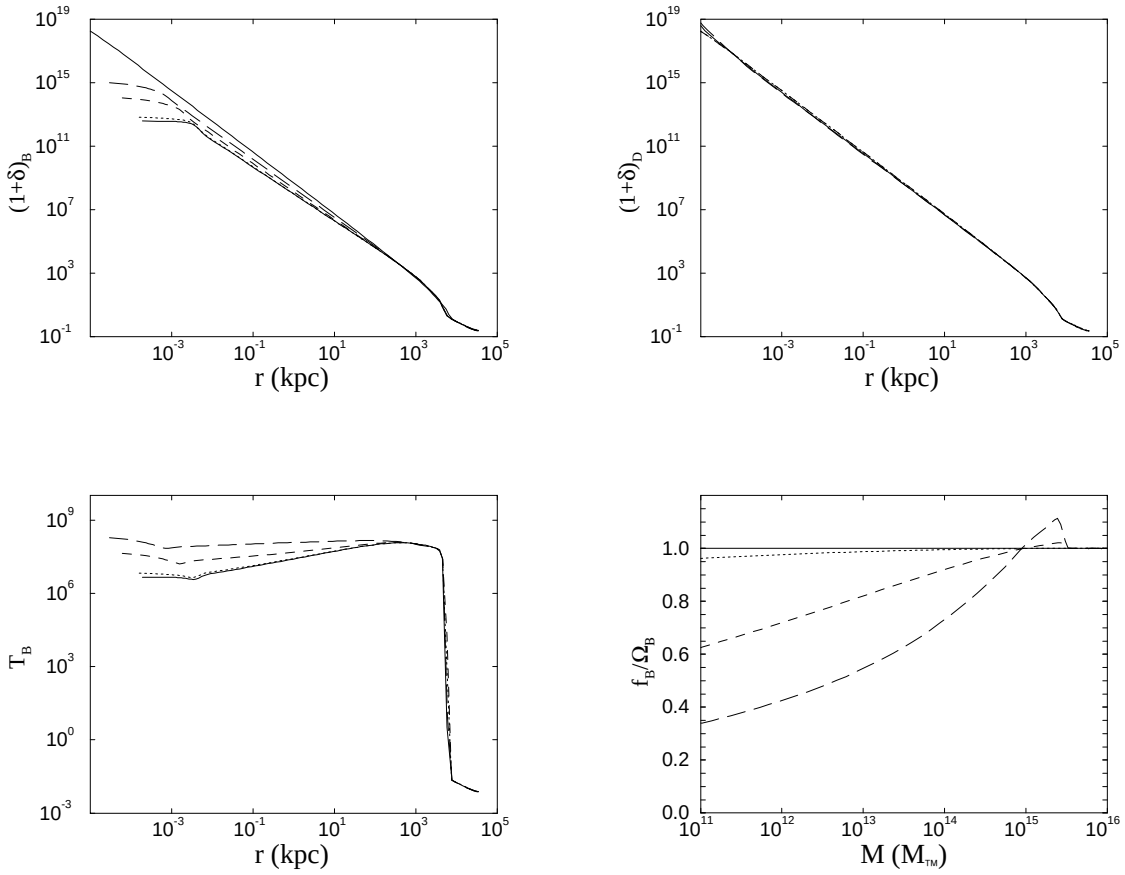

Fig. 4.— Dynamical structure of a spherical cluster at z = 0 with various Ω_B. (a) Gas over-density profiles for $\Omega_B = 1$ (solid line), 0.99 (dotted line), 0.9 (dashed line) and 0.01 (long-dashed line). We also plot for comparison the dark matter over-density profile obtained in the $\Omega_B = 0$ case (upper solid line). (b) Dark matter over-density profile for the same values of Ω_B. Note that all profiles are similar to the $\Omega_B = 0$ case. (c) Gas temperature for $\Omega_B = 1$, 0.99, 0.9 and 0.01. (d) Gas mass fraction versus total mass for $\Omega_B = 1$, 0.99, 0.9 and 0.01.

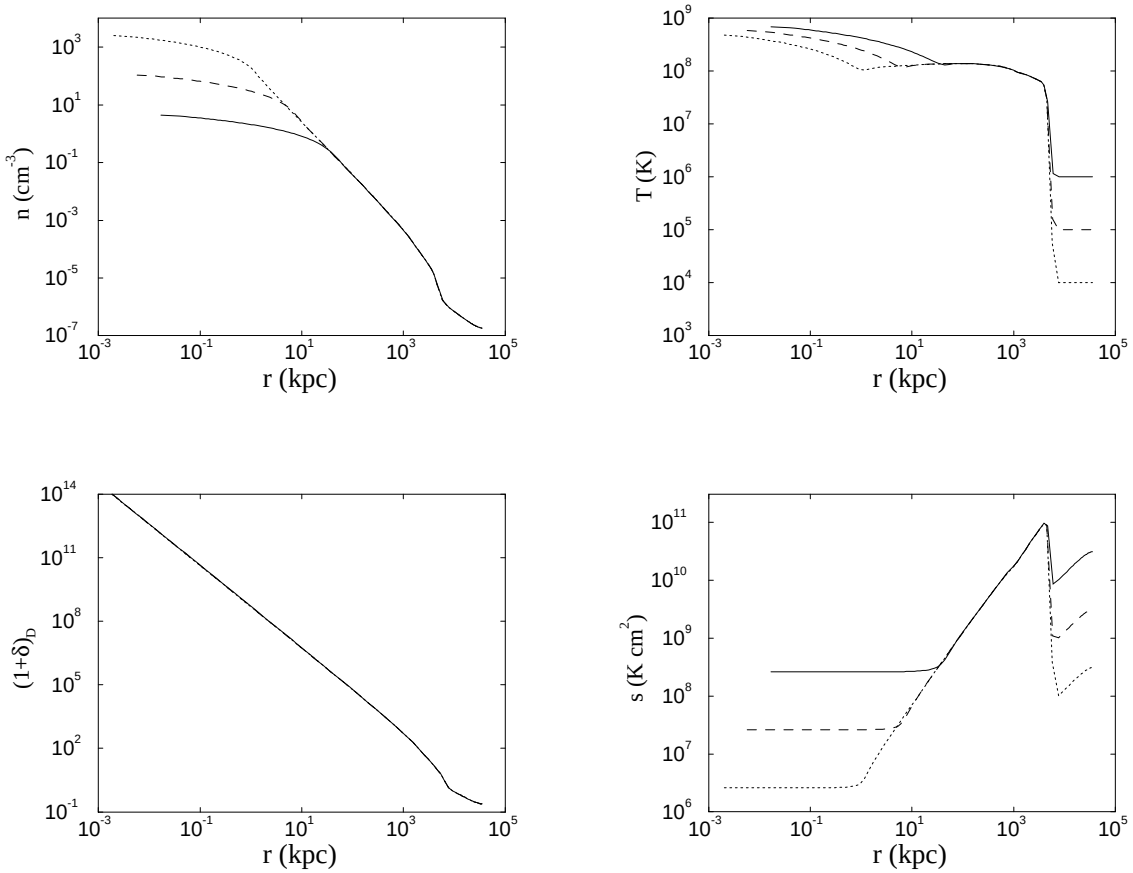

Fig. 5.— Dynamical structure of a spherical cluster ($M = 10^{16}\ M_\odot$ and $z_c = 2$) obtained at z = 0 for various initial entropy levels. The parameters are (see text) $T_{bg} = 10^4$ K (dotted line), 10^5 K (dashed line) and 10^6 K (solid line).